Sparsity-Promoting Estimator Design for Acceleration Sensor Placement in Civil Structures

A THESIS
SUBMITTED TO THE FACULTY OF THE GRADUATE SCHOOL
OF THE UNIVERSITY OF MINNESOTA
BY

Kali A. Gustafson

IN PARTIAL FULFILLMENT OF THE REQUIREMENTS
FOR THE DEGREE OF
MASTER OF SCIENCE

Dr. Lauren E. Linderman

May, 2019

Acknowledgements

I would like to express my sincere gratitude to my advisor, Professor Lauren Linderman, whose guidance and encouragement not only made this project possible but also convinced me of the possibility within myself. As a member of the Linderman Research Group, I quickly felt like I belonged. My physics background proved to be an asset in understanding structural dynamics and control, and it didn't take long before I felt I deserved the title of structural engineer.

I am appreciative of the strong support system I have found within the Department of Civil, Environmental, and Geo- Engineering, particularly in the structures group. Nicole, Sierra, Ramzi, Abraham, Ravi, Juan, and Jhenyffer have helped me get through the trying homework assignments and busy weeks that never seem to end. They have also helped keep me sane on a personal level, and their friendships are ones I hope to continue to cultivate after graduation.

Finally, I would like to acknowledge the continuous love and support of my family, without which I would not be where I am today. My mom and dad have never doubted my abilities and have always encouraged me to pursue my dreams. My sister never fails to put a smile on my face. In a world full of variables, mathematical and other, Ben has been my constant. His love, patience, and ability to see the bigger picture give me strength. And of course I have to thank my Assistant Research Assistant, Mellby Agnes Hall Cooper Gustafson (Mellby for short, Mell for shorter, or Miss Mell which isn't shorter but she likes it), for teaching me that just about any problem can be solved with a good walk.

The College of Science and Engineering (CSE) Diversity of Views and Experiences (DOVE) Fellowship at the University of Minnesota has supported this research. Financial support has also been provided by the National Science Foundation award CAREER-1750225.

Abstract

Sensor networks aid in updating dynamic models for monitoring and in limiting the vibration response of structures under dynamic loading. However, the vast scale of civil systems makes it impossible to measure all degrees of freedom. Therefore, a limited number of measurements are leveraged to obtain a full set of state (e.g. displacement and velocity) responses through state estimation. Spatially sparse feedback, which limits the information as well as the number of sensors for feedback, requires the selection of essential measurements. The exact sensor placement problem considers all possible combinations of sensors, which presents computational challenges for systems with a large number of degrees of freedom. Through the use of benchmark structures, the Kalman filter alternating direction method of multipliers (kfadmm) algorithm is shown to systematically balance measurement sparsity and estimator error covariance in acceleration sensor selection. Compared to the exact method and the sequential sensor placement method, the kfadmm sensor selection approach results in similar sensor choices at only slightly higher estimation error and with fewer combinations considered. The kfadmm method does not require knowing the number of sensors *a priori*. Rather, the best number of sensors for a given application can be determined after looking at the increase in the cost function as sensors are removed from the system. Additionally, the impact of Kalman filter covariance weightings on sensor placement is explored.

Contents

List of Tables

List of Figures

Chapter 1

Introduction

1.1 Motivation of Research

Sensor networks allow us to understand and improve structural performance under dynamic loading. Sensors provide valuable information, which can be used to promote low-damage seismic design and sustain the long-term performance of structures. Sensor networks aid in limiting the vibration response of structures under dynamic loading and in updating dynamic models for monitoring. In structural control, integrating sensor and actuator networks in the design of civil structures can limit the vibration response under dynamic loading instead of dissipating energy through localized damage [Yao, 1998]. Feedback control systems measure the structure's response and compute a force that then is applied to counteract the measured vibration. In structural health monitoring, the measured structural response is used to assess the performance of a structure. For example, dynamic model updating is used to indicate potential damage or to identify critical fatigue levels before damage can occur [Van Der Linden et al., 2011].

Although the most information would be obtained by placing sensors everywhere, the vast scale of civil systems makes it impossible to measure all degrees of freedom. Thus, estimation is used to predict the complete structural response given limited measurements. In both applications, control and monitoring, a limited number of measurements are leveraged to obtain a full set of state (e.g. displacement and velocity) responses through state estimation. Sparse feedback, which limits the information as

well as the number of sensors for feedback, requires the selection of essential measurements. The sensor placement problem involves finding the optimal location of sensors that will yield the best information about the behavior of the system.

Although presented through a structural framework, the sensor selection problem is not unique to civil applications. Robotics, target tracking, and chemical plant control are among the fields in which sensor selection has been studied [Hinson, 2014, Joshi and Boyd, 2009, Kammer, 2005, Yao et al., 1992]. Each application seeks the selection of an optimal measurement set to capture information regarding a desired system behavior.

A number of different optimization criteria have been considered in the selection problem formulation, including the observability Gramian [Hernandez, 2017, Hinson, 2014, Van Der Linden et al., 2011], estimation error covariance [Hernandez, 2017, Zhang and Xu, 2016], and Bayesian frameworks [Chen, 2013, Giraud and Jouvencel, 1995, Sun et al., 2015]. When the Kalman filter is used for state estimation, the minimum variance optimization criterion is utilized [Hernandez, 2017].

The exact sensor selection problem, which is a combinatorial problem, is cumbersome because it takes all possible combinations into account. Genetic algorithms [Abdullah et al., 2000, Tan et al., 2005, Yao et al., 1992] and sequential processes (forward and backward sequential sensor placement) [Hernandez, 2017, Papadimitriou, 2003] are two of the more common methods that have been studied to overcome the computational cost of the exact sensor placement problem.

The aforementioned approaches to the sensor placement problem are limited by their requirement to know the desired number of sensors before determining the selected set. The selected set refers to the number and location of sensors, both of which contribute to the degree of sub-optimality of the sensor selections. Previous approaches to sensor placement lack guidance regarding the number of sensors to be selected.

1.2 Overview of Research

The Kalman filter alternating direction method of multipliers (kfadmm) sensor selection method is proposed as a systematic approach for maximizing sensor sparsity and limiting the state estimation error covariance. In the kfadmm method, the objective function simultaneously optimizes minimum variance and measurement sparsity. Benchmark structures [Ohtori et al., 2004, Sun et al., 2016] are used to compare the kfadmm algorithm to the exact and sequential sensor placement methods. The kfadmm method

is shown to select similar sensors, require fewer combinations for computation, and provide useful information to determine a desired number of sensors compared to previous approaches to sensor selection. Ultimately, this research resulted in the proposal and validation of the kfadmm sensor selection method for acceleration sensor placement in civil structures.

The research presented herein is organized as follows.

- Chapter 2 presents a brief overview of some of the potential optimization criteria and previous sensor placement techniques that have been used to address the sensor placement problem.
- Chapter 3 provides the background theory, formulas, and tools used in this research. The lumped mass state-space system convention, discrete-time Kalman filter, and alternating direction method of multipliers are presented. Four benchmark structures used as comparison tools for estimator design approaches are also considered.
- Chapter 4 proposes the Kalman filter alternating direction method of multipliers (kfadmm) sensor selection method as a solution to the sensor placement problem. This chapter details the steps of the selection process and utilizes figures to allow for further understanding about how the algorithm is selecting sensors.
- Chapter 5 discusses considerations that were given to the building models and scaling used in implementation of the placement algorithms.
- Chapter 6 compares the kfadmm, exact, and sequential sensor placement methods. The impact of system scale (number of degrees of freedom) and model type (reduced-order and shear) are also accounted for in the relative sensor choices and effectiveness of the kfadmm method.
- Chapter 7 examines the effect of covariance weightings on sensor selection.
- Chapter 8 summarizes the conclusions of the thesis and recommendations for future research direction.

Chapter 2

Literature Review

This chapter introduces the traditional sensor placement problem, optimization criteria that have been studied, and sensor selection techniques.

2.1 The Sensor Placement Problem

To select sensors that will provide the best information about the system being studied, the traditional sensor placement problem requires placing m sensors in n possible locations. To determine the optimal sensor locations, the optimization criterion of each combination must be considered. The combination of sensors that best fits the optimization criterion is selected.

2.2 Optimization Criteria

In general, the selection optimization problem can be approached from one of two overarching frameworks: Bayesian or information theory [Joshi and Boyd, 2009].

The Bayesian framework is a probability-based approach that has recently been applied to the study of estimation and sensor placement. Chen provides an introductory-level review of Bayesian regularization as it relates to model estimation for linear dynamic systems [Chen, 2013]. In [Sun et al., 2015], a Bayesian inference-based regularization technique is presented to solve for unknown forces using incomplete output-only measurements from civil structures. Ultimately, simultaneous identification of structural parameters and unmeasured input forces is achieved through iterative minimization of

the difference between the measured and estimated data. Giraud and Jouvencel implement a Bayesian framework to address sensor selection in the design of sensor equipment (i.e. sensor choice and placement) and the management of information from a multi-sensor system (i.e. selection of necessary information) in the robotics field [Giraud and Jouvencel, 1995].

The information theory framework has been applied by numerous researchers. In [Kammer, 2005] and [Papadimitriou and Lombaert, 2012], the desired sensor choices are selected if they maximize a norm of the Fisher information matrix. Fisher information describes the amount of information available in a random measurement [Hinson, 2014]. Similarly, observability, i.e. how well the system states of displacement and velocity can be determined from system outputs, is also used as an optimization criterion for sensor placement in [Hernandez, 2017], [Hinson, 2014], and [Van Der Linden et al., 2011]. The observability Gramian, $\mathbf{W}$, is inversely proportional to the estimation covariance, and the eigenvalues of the observability Gramian describe the relative observabiltiy of each mode [Hinson, 2014]. Thus, the eigenvalues of the observability Gramian inversely control the estimation covariance [Hinson, 2014]. Table 2.1 summarizes the relationships between these measures. Hernandez concludes that use of the condition number of the observability Gramian as the criterion does not account for loading conditions, and as such, it may result in sub-optimal placement [Hernandez, 2017]. Hinson successfully uses an observability Gramian approach for sensor placement in nonlinear systems, including an underwater vehicle and an insect wing [Hinson, 2014]. Van Der Linden et. al. compare minimization of three information-based optimization criteria: inverse of the observability, static estimation error, and dynamic estimation error [Van Der Linden et al., 2011]. Using a model of the New Carquinez Bridge in California, the sensor selection results are shown to be similar for each criterion. The main difference between the optimization criteria considered is in the required computational effort. The dynamic estimation error, though it provided the most optimal results, required significantly more computation time. Another optimization criterion is the minimum variance approach [Hernandez, 2017, Zhang and Xu, 2016]. Because the Kalman filter is leveraged for state estimation, the optimization criterion implemented in the research in this thesis is the approach of minimizing the trace of the covariance matrix.

Table 2.1: Eigenvalue measures of the observability Gramian [Hinson, 2014]

measure	significance
$\lambda_{min}^{-1}(\mathbf{W})$	maximum estimation uncertainty
$\lambda_{max}^{-1}(\mathbf{W})$	minimum estimation uncertainty
$K(\mathbf{W})$	shape of estimation uncertainty ellipsoid
$\det[\mathbf{W}^{-1}]$	volume of estimation uncertainty ellipsoid
$\mathrm{tr}[\mathbf{W}^{-1}]$	average estimation uncertainty

2.3 Sensor Placement Techniques

The sensor placement problem can be solved through the exact placement method or approximation methods, including sequential placement algorithms and genetic algorithms.

2.3.1 Exact Placement Method

The exact placement method directly addresses the traditional sensor placement problem by considering all combinations of placing m sensors in n possible locations. The number of combinations considered is

$$\binom{n}{m} = \frac{n!}{m!(n-m)!} \tag{2.1}$$

This approach results in the best possible set of sensors for a given m and n; however, it presents computational challenges, especially for systems with a large number of degrees of freedom.

To select sensors for discrete-time systems, the system is first expressed in a lumped mass state-space form. The combination of sensors dictates the measurement output matrix rows, which contain information about each sensor in the combination. To configure m sensors, the posterior estimate error covariance matrix, $\mathbf{P}_{k|k}$, and corresponding Kalman gain matrix, $\mathbf{L}$, are computed. $\mathbf{P}_{k|k}$ and $\mathbf{L}$ provide information about the accuracy of the state (e.g. displacement or velocity) estimates and the sensors that are included in the estimation, respectively. The combination of sensors that minimizes the trace of the posterior estimate error covariance matrix corresponds to the optimal placement for a fixed number of m sensors.

2.3.2 Approximation Methods

To combat the computational cost of an exhaustive search, a variety of approximation methods have been utilized to address the sensor selection optimization problem. The main techniques that have been explored include forward and backward sequential sensor placement algorithms [Hernandez, 2017, Papadimitriou, 2003] and genetic algorithms [Abdullah et al., 2000, Tan et al., 2005, Yao et al., 1992].

Sequential Placement Algorithms

To configure m sensors, sequential sensor placement is a more computationally efficient method than the exact method [Hernandez, 2017]. In the sequential placement method, again in the context of the Kalman filter, the first of m sensors is placed optimally following the same procedure as the exact method. First, the posterior estimate error covariance matrix and corresponding Kalman gain matrix are calculated for each of the n possible sensor locations. The sensor that minimizes the trace of the posterior estimate error covariance matrix is selected. This first sensor's location is then fixed. Next, the second of m sensors is placed optimally in the remaining $n-1$ locations not filled by the first sensor. This process continues until m sensors have been placed. The combinatorial problem for sequential sensor placement becomes

$$\sum_{j=0}^{m-1}(n-j) \tag{2.2}$$

If one considers, for example, the problem of placing 3 sensors in 9 possible locations, the sequential method need only consider 24 combinations compared to the 84 required by the exact placement method.

This placement algorithm could be referred to as a forward sequential placement algorithm. For brevity, however, throughout this thesis, references to the sequential placement method will refer to the algorithm detailed above. The other type of sequential algorithm is a backward sequential placement algorithm, the details of which follow intuitively from the forward method. Backward sequential sensor selection starts with sensors placed at every possible measurement location. Sensors are then removed one-by-one until the desired m sensors remain. A sensor is removed when the inclusion of that sensor would increase the trace of the posterior error covariance matrix relative to the other options. When the number of sensors to be placed is small relative to

the number of degrees of freedom, forward sequential placement is less computationally expensive than its backward placement counterpart [Papadimitriou, 2003]. For this reason, the forward sequential placement method will be used for comparison in this work.

Genetic Algorithms

Genetic algorithms are probabilistic search procedures that attempt to increase the rate of convergence and thus decrease the computation time for the placement optimization problem [Abdullah et al., 2000]. Genetic algorithms are particularly powerful when working with discrete systems or when the function measuring performance is not continuous and differentiable [Tan et al., 2005]. This technique gets its name from the biological concept of natural selection, selecting sensors through an iterative process where only the "fittest" combinations proceed to the next iteration. The algorithm ends when a user-specified number of iterations is exceeded or when the average cost function is the same for a chosen number of iterations, whichever occurs first.

2.4 Summary

The traditional sensor placement problem, which results in an exact solution, can be computationally costly for systems with a large number of degrees of freedom. Thus, approximation methods have been introduced. Though they address the problem of finding optimal sensor locations, these previous methods of sensor selection do not provide insight into the optimal number of sensors. These challenges will be addressed with the proposed Kalman filter alternating direction method of multipliers (kfadmm) sensor selection method. Comparison to the exact and sequential placement methods will be used in this work to evaluate the proposed algorithm.

Chapter 3

Background

This chapter provides the technical background needed to understand the research presented herein. The tools used for state estimation, solving the state estimation optimization problem, and comparing sensor selection methods are discussed.

3.1 Lumped Mass System

The equation of motion for an n-story building structure can be written as

$$\mathbf{M}\,\ddot{\mathbf{x}}_{abs} + \mathbf{C}\,\dot{\mathbf{x}} + \mathbf{K}\,\mathbf{x} = \mathbf{u} \tag{3.1}$$

where $\mathbf{M}$, $\mathbf{C}$, and $\mathbf{K}$ are the $n \times n$ mass, damping, and stiffness matrices of the building system, respectively. $\mathbf{x}$ and $\dot{\mathbf{x}}$ are the displacement and velocity of each story relative to the ground, while $\ddot{\mathbf{x}}_{abs}$ is the absolute acceleration of each story. $\mathbf{u}$ is the control force input at each story. These vectors ($\ddot{\mathbf{x}}_{abs}$, $\dot{\mathbf{x}}$, $\mathbf{x}$, and $\mathbf{u}$) are $n \times 1$ vectors. The absolute acceleration can be written as a combination of the ground acceleration, $\ddot{\mathbf{x}}_g$, plus the acceleration relative to the ground, $\ddot{\mathbf{x}}$:

$$\ddot{\mathbf{x}}_{abs} = \ddot{\mathbf{x}}_g + \ddot{\mathbf{x}} \tag{3.2}$$

Thus, Equation 3.1 can be written as

$$\ddot{\mathbf{x}} = -\ddot{\mathbf{x}}_g - \mathbf{M}^{-1}\,\mathbf{K}\,\mathbf{x} - \mathbf{M}^{-1}\,\mathbf{C}\,\dot{\mathbf{x}} + \mathbf{M}^{-1}\,\mathbf{u} \tag{3.3}$$

The equation of motion can then be expressed in state-space form, which is convenient for numerical simulation in MATLAB and Simulink. The second-order differential equation is written as two first-order differential equations. Letting $\dot{\mathbf{x}}_1 = \dot{\mathbf{x}}$ and $\dot{\mathbf{x}}_2 = \ddot{\mathbf{x}}$, the state vector becomes

$$\begin{Bmatrix} \dot{\mathbf{x}}_1 \\ \dot{\mathbf{x}}_2 \end{Bmatrix} = \begin{bmatrix} \mathbf{0} & \mathbf{1} \\ -\mathbf{M}^{-1}\,\mathbf{K} & -\mathbf{M}^{-1}\,\mathbf{C} \end{bmatrix} \begin{Bmatrix} \mathbf{x}_1 \\ \mathbf{x}_2 \end{Bmatrix} + \begin{bmatrix} \mathbf{0} \\ \mathbf{M}^{-1} \end{bmatrix} \Big\{ \mathbf{u} \Big\} + \begin{bmatrix} \mathbf{0} \\ -\mathbf{1} \end{bmatrix} \Big\{ \ddot{\mathbf{x}}_g \Big\} \tag{3.4}$$

The measurement vector, which contains relative displacement and velocity as well as absolute acceleration sensor measurements for each of the n degrees of freedom (floors) of the structure, can likewise be written as

$$\Big\{ \mathbf{y} \Big\} = \begin{Bmatrix} \mathbf{x} \\ \dot{\mathbf{x}} \\ \ddot{\mathbf{x}}_{abs} \end{Bmatrix} = \begin{bmatrix} \mathbf{1} & \mathbf{0} \\ \mathbf{0} & \mathbf{1} \\ -\mathbf{M}^{-1}\,\mathbf{K} & -\mathbf{M}^{-1}\,\mathbf{C} \end{bmatrix} \begin{Bmatrix} \mathbf{x}_1 \\ \mathbf{x}_2 \end{Bmatrix} + \begin{bmatrix} \mathbf{0} \\ \mathbf{0} \\ \mathbf{M}^{-1} \end{bmatrix} \Big\{ \mathbf{u} \Big\} + \begin{bmatrix} \mathbf{0} \\ \mathbf{0} \\ \mathbf{0} \end{bmatrix} \Big\{ \ddot{\mathbf{x}}_g \Big\} \tag{3.5}$$

Equations 3.4 and 3.5 can be written in a condensed format as

$$\begin{aligned} \dot{\mathbf{x}} &= \mathbf{A}\,\mathbf{x} + \mathbf{B}\,\mathbf{u} + \mathbf{E}\,\ddot{\mathbf{x}}_g \\ \mathbf{y} &= \mathbf{C}\,\mathbf{x} + \mathbf{D}\,\mathbf{u} + \mathbf{F}\,\ddot{\mathbf{x}}_g \end{aligned} \tag{3.6}$$

However, in this application, a discrete-time Kalman filter is used for state estimation. Therefore, the discrete-time state-space representation of the structural system is implemented:

$$\begin{aligned} \mathbf{x}[k+1] &= \mathbf{A}\,\mathbf{x}[k] + \mathbf{B}\,\mathbf{u}[k] + \mathbf{E}\,\ddot{\mathbf{x}}_g[k] \\ \mathbf{y}[k] &= \mathbf{C}\,\mathbf{x}[k] + \mathbf{D}\,\mathbf{u}[k] + \mathbf{F}\,\ddot{\mathbf{x}}_g[k] \end{aligned} \tag{3.7}$$

where $\mathbf{x} \in \mathbb{R}^n$ are the states of the system, $\mathbf{u} \in \mathbb{R}^p$ are the system control inputs, $\ddot{\mathbf{x}}_g$ is the ground acceleration input, and $\mathbf{y} \in \mathbb{R}^m$ are the measurements at each step $k \in \mathbb{N}$ for $t = \Delta T\,k$ where ΔT is the sample time. $\mathbf{A}$ is the $n \times n$ state transition matrix, $\mathbf{B}$ is the $n \times p$ control input matrix, $\mathbf{E}$ is the $n \times 1$ ground input matrix, $\mathbf{C}$ is the $m \times n$ measurement output matrix, $\mathbf{D}$ is the $m \times p$ control feedforward matrix, and $\mathbf{F}$ is the $m \times 1$ ground feedforward matrix. The pair $(\mathbf{A}, \mathbf{C})$ is observable. For the purposes of this thesis, the measurements considered, $\mathbf{y}$, are only acceleration measurement outputs.

3.2 Discrete-time Kalman Filter

In a structural control application, sensor measurements of the structural response are used as feedback to compute a force that will ultimately limit the vibration. The complete feedback control loop combines an estimator and controller, as can be seen in Figure 3.1. The estimator determines the full state from limited measurements (e.g. acceleration only), and the controller computes the desired control command based on the full state estimate. As the estimator links the measurements and the control command, the estimator is leveraged within the sensor selection process.

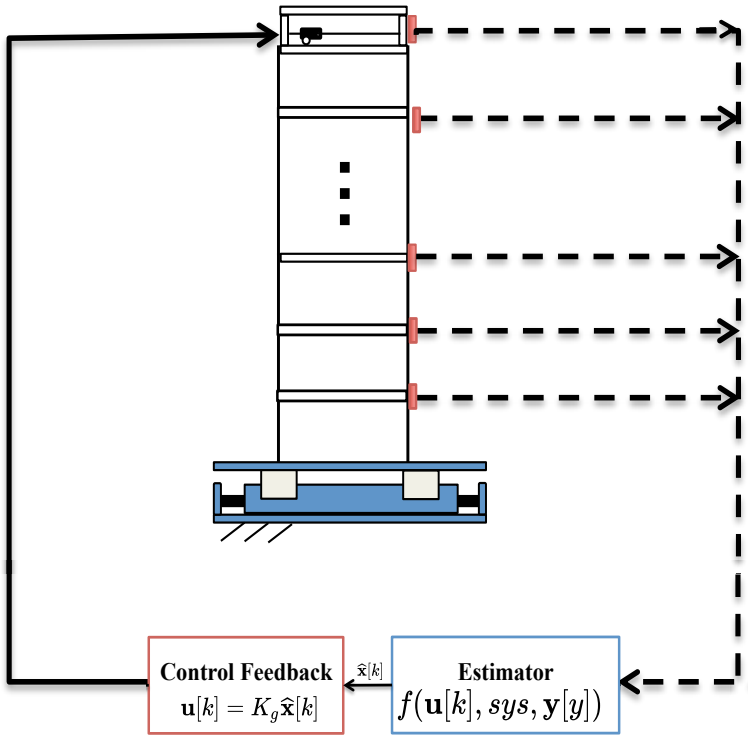

Figure 3.1: Sample control feedback loop for a building equipped with sensors and an actuator

The goal of the Kalman estimator is to minimize the posterior estimate error covariance matrix:

$$\begin{aligned}\mathbf{P}_{k|k} &= E[(\mathbf{x}[k] - \hat{\mathbf{x}}[k])\,(\mathbf{x}[k] - \hat{\mathbf{x}}[k])^{\mathrm{T}}] \\ &= E[(\mathbf{e}[k]\,\mathbf{e}[k])^{\mathrm{T}}]\end{aligned} \tag{3.8}$$

where $\mathbf{x}[k]$ is the state, $\hat{\mathbf{x}}[k]$ is the estimated state, and $\mathbf{e}[k]$ is the error at step k. The

resulting solution for the Kalman filter is the Kalman gain, $\mathbf{L}$, which is a fully-populated n by m matrix where n is the number of states and m is the number of measurements.

To calculate the time-varying Kalman gain in discrete-time, the following iterations are made [Thacker and Lacey, 1998]:

$$\begin{aligned}
\mathbf{L} &= \mathbf{P}'_{k|k}\,\mathbf{C}^{\mathrm{T}}(\mathbf{C}\,\mathbf{P}'_{k|k}\,\mathbf{C}^{\mathrm{T}} + \mathbf{R})^{-1} \\
\hat{\mathbf{x}}[k] &= \hat{\mathbf{x}}'[k] + \mathbf{L}(\mathbf{C}\,\mathbf{x}[k] - \mathbf{C}\,\hat{\mathbf{x}}'[k] + \mathbf{v}) \\
\mathbf{P}_{k|k} &= (\mathbf{I} - \mathbf{L}\,\mathbf{C})\mathbf{P}'_{k|k} \\
\hat{\mathbf{x}}'[k+1] &= \mathbf{A}\,\hat{\mathbf{x}}[k] \\
\mathbf{e}'[k+1] &= \mathbf{x}[k+1] - \hat{\mathbf{x}}'[k+1] \\
&= (\mathbf{A}\,\mathbf{x}[k] + \mathbf{w}) - \mathbf{A}\,\hat{\mathbf{x}}[k] \\
&= \mathbf{A}\,\mathbf{e}[k] + \mathbf{w} \\
\mathbf{P}'_{k+1|k+1} &= E[(\mathbf{e}'[k+1]\,\mathbf{e}'[k+1])^{\mathrm{T}}] \\
&= \mathbf{A}\,\mathbf{P}_{k|k}\,\mathbf{A}^{\mathrm{T}} + \mathbf{Q}
\end{aligned} \tag{3.9}$$

where the prime ($'$) superscript indicates the prior iteration. The measurement noise, $\mathbf{v}$, and process noise, $\mathbf{w}$, are assumed to be independent zero-mean Gaussian white noise with covariances $\mathbf{R}$ and $\mathbf{Q}$. For a linear time-invariant system, the time-varying Kalman gain will approach the infinite-horizon steady-state gain.

3.3 Alternating Direction Method of Multipliers (ADMM)

The alternating direction method of multipliers (ADMM) algorithm is used to solve the objective function in the proposed Kalman filter alternating direction method of multiplier (kfadmm) sensor selection method. The dual optimization problem is solved by expanding on the ADMM steps outlined by Lin et. al. [Lin et al., 2013].

The first step is to represent the discrete-time Kalman gain matrix, $\mathbf{L}$ from Equation 3.9, as the matrices $\mathbf{L}$ and $\mathbf{G}$ and apply a constraint:

$$\begin{aligned}
&\underset{\mathbf{L},\mathbf{G}}{\text{minimize}} && \mathbf{J}(\mathbf{L}) + \gamma\,\mathbf{g}(\mathbf{G}) \\
&\text{subject to} && \mathbf{L} - \mathbf{G} = \mathbf{0}
\end{aligned} \tag{3.10}$$

Note that Equation 3.10 is equivalent to the objective function for the kfadmm sensor

selection method; however, in this form, the objective function is decoupled to simplify the solution.

An augmented Lagrangian, $\mathcal{L}_\rho$, is introduced following Equation 3.10:

$$\mathcal{L}_\rho\left(\mathbf{L},\mathbf{G},\mathbf{\Lambda}\right)=\mathbf{J}(\mathbf{L})+\gamma\,\mathbf{g}(\mathbf{G})+\operatorname{tr}\left(\mathbf{\Lambda}^{\mathrm{T}}(\mathbf{L}-\mathbf{G})\right)+\frac{\rho}{2}\left\|\mathbf{L}-\mathbf{G}\right\|_F^2 \tag{3.11}$$

where $\mathbf{\Lambda}$ is the Lagrange multiplier matrix, ρ is a positive scalar parameter that scales the solution path, and $\|\cdot\|_F$ is the Frobenius norm. The matrices $\mathbf{L}^k$, $\mathbf{G}^k$, and $\mathbf{\Lambda}^k$ are initialized using

$$\mathbf{L}^0=\mathbf{L}_{DTKF},\quad \mathbf{G}^0=\mathbf{L}_{DTKF},\quad \mathbf{\Lambda}^0=\mathbf{0} \tag{3.12}$$

where $\mathbf{L}_{DTKF}$ refers to the discrete-time Kalman filter gain for full measurement feedback. Then, the solution to Equation 3.10 is obtained through a sequence of iterations

$$\mathbf{L}^{k+1}:=\arg\min_{\mathbf{L}}\ \mathcal{L}_\rho\left(\mathbf{L},\mathbf{G}^k,\mathbf{\Lambda}^k\right) \tag{3.13a}$$

$$\mathbf{G}^{k+1}:=\arg\min_{\mathbf{G}}\ \mathcal{L}_\rho\left(\mathbf{L}^{k+1},\mathbf{G},\mathbf{\Lambda}^k\right) \tag{3.13b}$$

$$\mathbf{\Lambda}^{k+1}:=\mathbf{\Lambda}^k+\rho\left(\mathbf{L}^{k+1}-\mathbf{G}^{k+1}\right) \tag{3.13c}$$

The L-minimization (Equation 3.13a) is solved for each iteration by calculating

$$\mathbf{L}=(\mathbf{P}'_{k|k}\,\mathbf{C}^{\mathrm{T}}+\rho\,\mathbf{U})(\mathbf{C}\,\mathbf{P}'_{k|k}\,\mathbf{C}^{\mathrm{T}}+\mathbf{R}+\rho\,\mathbf{I})^{-1} \tag{3.14}$$

where

$$\mathbf{U}^{k+1}=\mathbf{G}^k-\frac{\mathbf{\Lambda}^k}{\rho} \tag{3.15}$$

and Equation 3.14 is the same as the first step in calculating the Kalman gain matrix (Equation 3.9) except for the addition of the offsets marked with ρ.

The G-minimization for each iteration (Equation 3.13b), which is made possible by the separability of $\mathbf{L}$ and $\mathbf{G}$, considers column-wise minimization of

$$\gamma\,\mathbf{g}(\mathbf{G}_m)+\frac{\rho}{2}\left(\mathbf{G}_m-\mathbf{V}_m\right)^2 \tag{3.16}$$

where m refers to the column index (measurement location). This work focused on

implementation of the cardinality function for $\mathbf{g}(\mathbf{G}_m)$:

$$\mathbf{g}(\mathbf{G}_m) = \text{card}\left(\|\mathbf{G}_m\|_2\right), \quad \text{card}\left(\|\mathbf{G}_m\|_2\right) = \left\{ \begin{array}{ll} 1, & \mathbf{G}_m \neq \mathbf{0} \\ 0, & \mathbf{G}_m = \mathbf{0} \end{array} \right\} \tag{3.17}$$

The cardinality function truncates the gain matrix column-wise, a non-convex optimization problem. The gain matrix columns are truncated as follows:

$$\mathbf{G}_m = \left\{ \begin{array}{ll} \mathbf{V}_m, & \gamma < \frac{\rho}{2} \|\mathbf{V}_m\|_2^2 \\ \mathbf{0}, & \gamma \geq \frac{\rho}{2} \|\mathbf{V}_m\|_2^2 \end{array} \right\} \tag{3.18}$$

where $\|\cdot\|_2$ is the Euclidean norm and

$$\mathbf{V}^{k+1} = \mathbf{L}^{k+1} + \frac{\mathbf{\Lambda}^k}{\rho} \tag{3.19}$$

Finally, the Lagrange multiplier matrix (Equation 3.13c) is updated for the current iteration:

$$\mathbf{\Lambda}^{k+1} = \mathbf{\Lambda}^k + \rho\left(\mathbf{L}^{k+1} - \mathbf{G}^{k+1}\right) \tag{3.20}$$

Equations 3.13a, 3.13b, and 3.13c iterate, and the ADMM process is completed as $\mathbf{\Lambda}^{k+1}$ approaches zero. The final gain matrix $\mathbf{L}^{k+1}$ dictates the ultimate sensor selections, updating the gain and estimate error covariance for each γ in a final polishing step.

3.4 Benchmark Structures for Control of Civil Systems

The use of benchmark structures allows for straightforward comparison of various structural control strategies. The 3-story wireless benchmark by Sun et. al. was designed to capture features in addition to the structural dynamics of a building instrumented with a wireless network [Sun et al., 2016]. Brandow and Johnston Associates designed the 3-, 9-, and 20- story nonlinear benchmark structures for the SAC Phase II Steel Project [Ohtori et al., 2004].

3.4.1 3-story Wireless Benchmark

The 3-story wireless benchmark structure consists of three floors plus an active mass driver (AMD) system that is placed on the top floor. An AMD is one type of structural

control device that can be implemented to provide the desired counter-force to building excitation. In this structure, the first three modes occur at 5.81, 17.68, and 28.53 Hz. The scaled model provided allows for selection of the absolute acceleration measurements from each of the three floors and the AMD.

3.4.2 3-story Nonlinear Benchmark

The 3-story nonlinear benchmark was designed to represent a typical low-rise steel building in the Los Angeles area for the SAC project. The building contains four bays in the N-S direction and six bays in the E-W direction. The first three natural frequencies for the 3-story benchmark are 0.99, 3.06, and 5.83 Hz.

3.4.3 9-story Nonlinear Benchmark

The 9-story steel building is a typical mid-rise structure designed for the SAC project. It consists of five bays in both the N-S and E-W directions. The building also has a single-floor basement. The first three modes occur at 0.443, 1.18, and 2.05 Hz. The building is excited at the ground level, and acceleration measurements of each of the nine above-ground floors are considered. The reduced-order model of this 9-story nonlinear benchmark structure developed by Ohtori et. al. [Ohtori et al., 2004] was used to evaluate the kfadmm selection algorithm in the following chapters.

3.4.4 20-story Nonlinear Benchmark

The 20-story steel building is the third and final benchmark structure designed for the SAC project, representing a typical high-rise building for the Los Angeles region. There are five bays in the N-S direction and six bays in the E-W. The building also contains two floors below-ground. Its first five natural frequencies are 0.261, 0.753, 1.30, 1.83, and 2.40 Hz.

3.5 Summary

This chapter details the discrete-time Kalman filter and the alternating direction method of multipliers, the two key components of the proposed Kalman filter alternating direction method of multipliers (kfadmm) sensor selection method. Application of these algorithms to the sensor selection problem, as will be shown in the following chapters,

allows for efficient calculation and comparison of the different sensor selections through the γ-parameterized gain matrices. The four benchmark building structures will be integrated to compare the sensor placement algorithms studied. However, the 9-story benchmark will be the focus of the work presented.

Chapter 4

kfadmm Sensor Selection Method

This chapter presents the Kalman filter alternating direction method of multipliers (kfadmm) sensor selection method and depicts how the algorithm makes its sensor choices.

4.1 Proposed Algorithm

The algorithm presented in this section aims to select sensors in a more systematic framework than an exhaustive consideration of all possible sensor combinations. This method is extended from existing sparse feedback control approaches that permit a convex relaxation of the original problem [Joshi and Boyd, 2009, Lin et al., 2013]. In the proposed optimization, a column sparsity-promoting penalty function is included in the function to be minimized as a part of the estimator design. No assumptions of the sparse form are made *a priori*.

The objective function is given as

$$\underset{\mathbf{L}}{\text{minimize}} \quad \mathbf{J}(\mathbf{L}) + \gamma\, \mathbf{g}(\mathbf{L}) \tag{4.1}$$

where $\mathbf{J}(\mathbf{L})$ is the cost function, γ is the sparsity parameter, and $\mathbf{g}(\mathbf{L})$ is the penalty function. The cost function is the same as for the discrete-time Kalman filter:

$$\mathbf{J}(\mathbf{L}) = \frac{1}{2} \operatorname{tr}\left(\mathbf{P}_{k|k}\right) \tag{4.2}$$

where $\mathbf{P}_{k|k}$ is the posterior error covariance (Equation 3.8). The goal is to reduce the

number of measurements, so the penalty function, $\mathbf{g}(\mathbf{L})$, emphasizes column sparsity of the Kalman gain matrix, $\mathbf{L}$, through the cardinality function:

$$\mathbf{g}(\mathbf{L}) = \text{card}\left(\|\mathbf{L}_1\|_2, \|\mathbf{L}_2\|_2, ..., \|\mathbf{L}_m\|_2 \right) \tag{4.3}$$

where the subscript of $\mathbf{L}$ is the corresponding column vector. If γ equals zero, the algorithm returns the original discrete-time Kalman estimator gain. As the sparsity parameter increases, the column sparsity of the Kalman gain matrix increases and the required measurement feedback reduces. The alternating direction method of multipliers (Section 3.3) is used to solve the dual optimization problem.

Figure 4.1 illustrates the balance between optimizing sensor sparsity and estimate error covariance outlined in the objective function (Equation 4.1). As the sparsity parameter, γ, increases, the number of sensors decreases but the covariance estimation error increases. This result makes intuitive sense: for full sensor feedback, the estimation error is at its minimum because the most information possible is used for estimation; however, as the number of sensors decreases so does the information used for state estimation, resulting in increased estimation error.

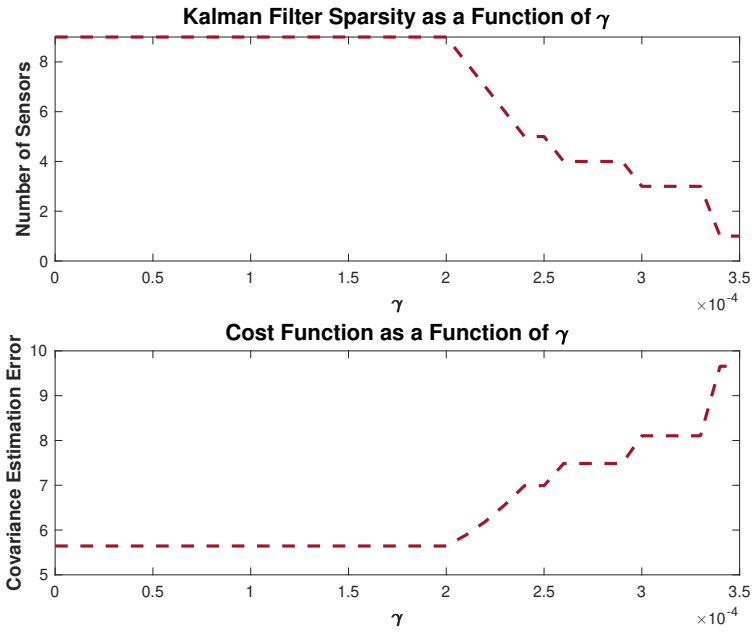

Figure 4.1: Sparsity and cost as a function of γ for the 9-story nonlinear benchmark structure

4.2 Visualization Through the 9-story Nonlinear Benchmark Structure

For the kfadmm algorithm, sensor selection is determined through analysis of the Kalman gain matrix, $\mathbf{L}$. Each column of the gain matrix corresponds to a potential measurement location. In the 9-story benchmark these measurement locations are the floors of the structure. A ribbon plot of the gain matrix for the 9-story nonlinear benchmark structure is shown in Figure 4.2, where each measurement location is depicted as a different color strip. To determine the sensor selection, the kfadmm algorithm quantifies the contribution of each floor with the penalty function, $\mathbf{g}(\mathbf{L})$, which considers the Euclidean norm of each column of the Kalman gain matrix. Measurement locations with smaller Euclidean norms are eliminated from feedback as the sparsity parameter, γ, increases. In Figure 4.3, the Euclidean norm for each column (floor) of the Kalman gain is plotted. With this information, the sensor selection results from the kfadmm algorithm are understood: for m sensors, one would choose the m floors with the largest Euclidean norms. For example, for three sensor measurements, one would select floors 9, 2, and 1.

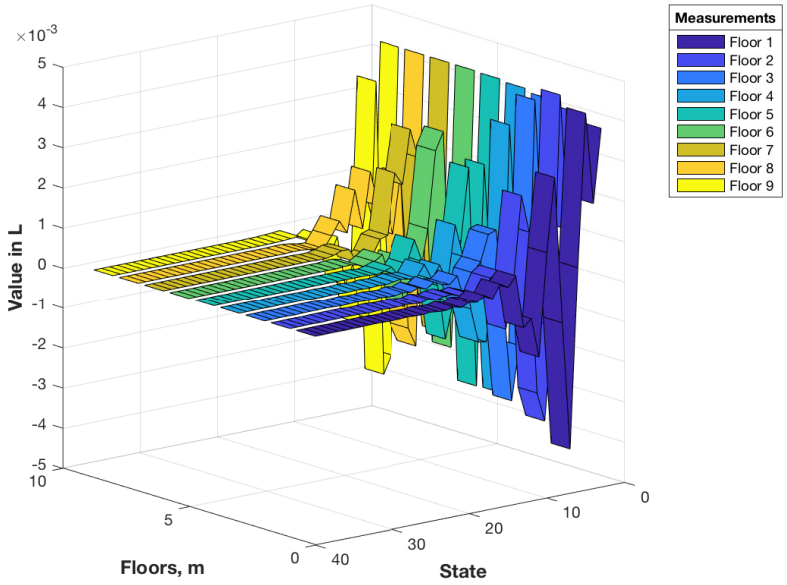

Figure 4.2: Ribbon plot of the Kalman gain matrix, $\mathbf{L}$, for full acceleration measurement feedback

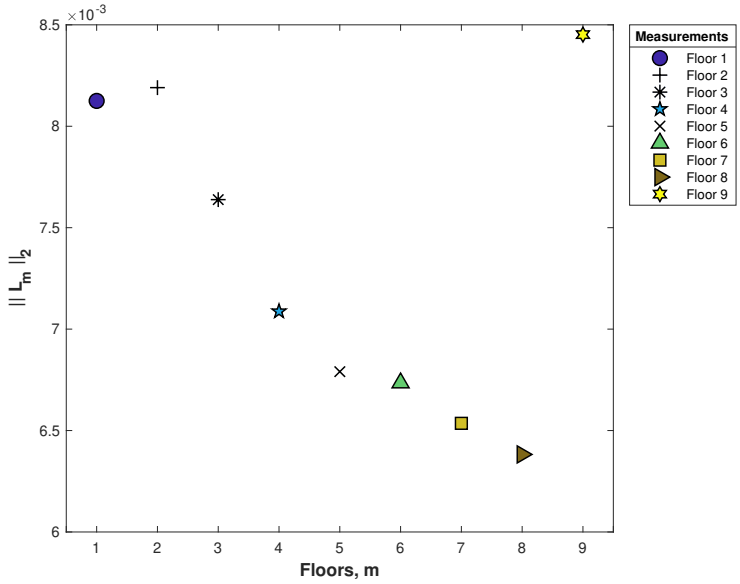

Figure 4.3: Euclidean norm of each column (floor) of the Kalman gain matrix for full acceleration measurement feedback

The sensor selection results for the numerical investigation of the kfadmm algorithm when it was applied to the 9-story nonlinear benchmark structure are summarized in Table 4.1. For this example, γ was chosen as $[0 : 1 * 10^{-5} : 3.5 * 10^{-4}]$ and the measurement noise was assumed to be greater than the process noise, $\mathbf{Q}/\mathbf{R} < 1$ ($\mathbf{Q}/\mathbf{R} = 0.1$). The selection parallels that in Figure 4.1, going from the full measurements to measuring just the 9th story as sparsity is increased.

Table 4.1: Acceleration sensor selection results assuming $\mathbf{Q}/\mathbf{R} < 1$ for the 9-story nonlinear benchmark structure

No. of Sensors	Selection (Floors)							
8	9	7	6	5	4	3	2	1
7	9		6	5	4	3	2	1
6	9			5	4	3	2	1
5	9				4	3	2	1
4	9					3	2	1
3	9						2	1
1	9							

Note that the kfadmm placement method did not select a combination of two sensors. The hypothesis behind this result is that the Euclidean norms of the columns corresponding to floors 1 and 2 were so similar the algorithm did not differentiate between them for the employed γ range.

Chapter 5

Sensitivity to Models and Scaling

The kfadmm sensor selection method was applied to multiple models in order to assess how the scale of the system and model type impact algorithm performance. Furthermore, the importance of scaling to maintain an accurate representation of the dominant system dynamics within the optimization process was established.

5.1 Models Considered

The reduced-order 3-, 9-, and 20- story nonlinear benchmark models [Ohtori et al., 2004] were considered in the evaluation of the proposed sparsity-promoting algorithm. The 3-story wireless benchmark [Sun et al., 2016] was evaluated, too. The model type may also have a significant impact on the sensor selection. As a result, in addition to the reduced-order models, the 3-, 9-, and 20- story nonlinear benchmark models were evaluated as shear models by eliminating the vertical and rotational degrees of freedom, fixing the structure at the ground level, and linking the horizontal degrees of freedom for each floor. To give an idea of the breadth of the results presented, Chapter 6 expands on a couple of the models considered. The selection results from all of the models follow the patterns in placement and number of required function evaluations outlined in the body of this thesis. Appendix A details the comparison of sensor selection results for the exact, sequential, and kfadmm methods when applied to the various models considered.

5.2 Importance of Scaling

For application of the kfadmm algorithm, the models need to be scaled in order to obtain accurate results. The widespread values of the original, unscaled, models likely create issues for inversion within kfadmm.

The observability Gramian of the different models considered supports this conclusion related to scaling. Recall in Equation 3.7 the pair $(\mathbf{A}, \mathbf{C})$ is assumed to be observable. Observability is a prerequisite of the state estimation problem. An observable state is one that can be determined from the inputs and outputs of a system: the goal of the state estimation problem. The observability Gramian for a discrete linear time-invariant system is calculated as

$$\mathbf{W}[k-1] = \sum_{s=0}^{k-1} (\mathbf{A}^{\mathrm{T}})^s \, \mathbf{C}^{\mathrm{T}} \, \mathbf{C} \, \mathbf{A}^s \tag{5.1}$$

The condition number of the observability Gramian corresponds to the shape of the estimation uncertainty ellipsoid [Hinson, 2014]. A well-conditioned system will have an equitable distribution of output energies and thus a more spherical shape. A poorly conditioned system will have some modes that dominate others, which creates an ellipsoid. A poorly-conditioned system can be identified by a large condition number. When the kfadmm algorithm was run for systems without prior scaling, the condition numbers of the observability Gramians were orders of magnitude greater than those of the scaled systems.

Because the kfadmm selection algorithm was coded outside of MATLAB's Control System Toolbox$^{\mathrm{TM}}$ [The MathWorks, Inc., 2018], it was necessary to scale the building models to ensure the computations were performed on a well-scaled system, that is, a system in which the state space matrices in Equation 3.7 were similar in magnitude and not sensitive to small entries. These small entries make the optimization for sensor selection challenging. To accomplish this scaling before running kfadmm, the "prescale" function was used to maximize accuracy of the frequency-domain analysis over the dominant frequency band.

Chapter 6

Comparison of Sensor Selection Algorithms

To understand the benefits and trade-offs of the kfadmm algorithm for sensor selection, this chapter compares the kfadmm method to an exhaustive search of all possible sensor combinations and the sequential sensor placement approximation technique.

6.1 Comparison Through the 9-story Nonlinear Benchmark Structure

The acceleration sensor selection results for the exact, sequential, and kfadmm algorithms applied to the 9-story nonlinear benchmark structure are given in Table 6.1. When selecting 7, 6, 5, 2, and 1 sensors, the exact and sequential results matched exactly. All three methods matched in their selection of 1 sensor, selecting the 9th floor.

As expected, for a certain number of sensors, m, the trace of the posterior error covariance matrix was slightly larger when calculated with the kfadmm selections than with the exact or sequential selections. This result is shown in Figure 6.1. Table 6.2 presents the percent differences of the cost function for the two approximation methods when compared with the exact method. The sequential method selections were closer to the exact method's selections than the kfadmm selections were; however, the percent difference for every kfadmm selection was less than four percent higher than the exact selection.

The key difference between the three methods considered for sensor selection is

that for kfadmm the number of m sensors is not required *a priori*. With the kfadmm approach, one has the ability to determine the best m for a given application after looking at the increase in the cost function, $\mathrm{tr}\,(\mathbf{P}_{k|k})$, as more sensors are removed from the system. Thus, this improved insight on the sensor selection approach is worth the anticipated trade-off in optimality.

Computationally, the sequential and kfadmm methods lower the number of combinations that must be considered for most selections when compared to the exact method. Table 6.3 summarizes the number of function evaluations considered for each method when applied to the 9-story nonlinear benchmark structure. The sparsity parameter, γ, for kfadmm is equivalent to the combinatorial problems discussed for the exact and sequential approaches in Equations 2.1 and 2.2. Since the user has control over the sparsity parameter, a coarser or finer range of γ values, i.e. a larger or smaller number of function evaluations, could be used depending on the detail desired for the application. As a result, the given number of kfadmm combinations in Table 6.3 could vary. Appendix B provides an example of a coarser γ range applied to the 9-story structure where the kfadmm algorithm results in fewer function evaluations than both the exact and sequential methods. Note that the number of kfadmm combinations presented in Table 6.3 corresponds to the level of selection detail presented in Table 6.1 and Figure 4.1. Moreover, the exact and sequential methods would require 474 and 223 evaluations respectively to get the same information kfadmm obtained in 35 evaluations, since m was not required *a priori* for kfadmm and the results automatically followed for selecting 1, 3, 4, 5, 6, 7, and 8 sensors.

Table 6.1: Comparison of acceleration sensor selection results, assuming $\mathbf{Q}/\mathbf{R} < 1$ ($\mathbf{Q}/\mathbf{R} = 0.1$), for the exact, sequential, and kfadmm methods applied to the 9-story nonlinear benchmark structure

Method		Exact Selection (Floors)	Sequential Selection (Floors)	kfadmm Selection (Floors)
No. of Sensors	**8**	9 8 7 6 4 3 2 1	9 8 7 6 5 3 2 1	9 7 6 5 4 3 2 1
	7	9 8 6 5 3 2 1	9 8 6 5 3 2 1	9 6 5 4 3 2 1
	6	9 8 6 5 3 2	9 8 6 5 3 2	9 5 4 3 2 1
	5	9 8 6 3 2	9 8 6 3 2	9 4 3 2 1
	4	9 8 3 2	9 8 6 3	9 3 2 1
	3	9 8 2	9 6 3	9 2 1
	2	9 6	9 6	
	1	9	9	9

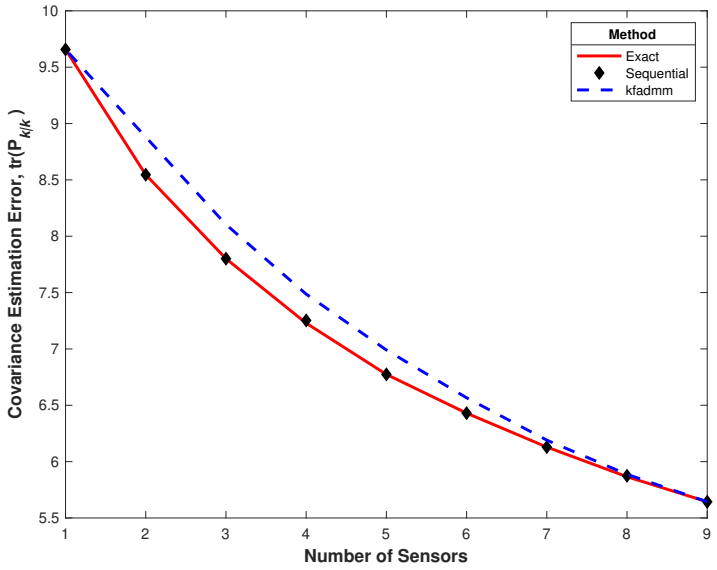

Figure 6.1: $\mathrm{tr}\,(\mathbf{P}_{k|k})$ versus number of acceleration sensors, assuming $\mathbf{Q}/\mathbf{R} < 1$, for the exact, sequential, and kfadmm methods applied to the 9-story nonlinear benchmark structure

Table 6.2: $\mathrm{tr}\,(\mathbf{P}_{k|k})$ percent difference comparison with the exact method for acceleration sensor selections made with the sequential and kfadmm methods, assuming $\mathbf{Q}/\mathbf{R} < 1$ for the 9-story nonlinear benchmark structure

Method	$\mathrm{tr}\,(\mathbf{P}_{k\|k})$ Percent Difference for **No.** of Sensors						
	8	**7**	**6**	**5**	**4**	**3**	**1**
Sequential	0.147	0	0	0	0.334	0.003	0
kfadmm	0.361	0.996	2.097	3.143	3.502	3.813	0

Table 6.3: Comparison of number of function evaluations for a certain number of selected acceleration sensors, assuming $\mathbf{Q}/\mathbf{R} < 1$, for the exact, sequential, and kfadmm methods applied to the 9-story nonlinear benchmark structure

Method	Function Evaluations for **No.** of Sensors							**Total**
	8	**7**	**6**	**5**	**4**	**3**	**1**	**Evaluations**
Exact	9	36	84	126	126	84	9	474
Sequential	44	42	39	35	30	24	9	223
kfadmm	22	23	24	25	27	31	35	35

6.2 Impact of System Scale

In general, the system scale (number of degrees of freedom) did not impact the patterns in sensor placement observed. The detailed sensor selection results for the other models considered can be found in Appendix A. Independent of the structural system scale, comparison of the kfadmm method with the other sensor selection methods considered led to the following conclusions:

1. Both the 9- and 20-story benchmark results showed less error in the selections made by the sequential method than the selections made by kfadmm (Tables 6.2 and 6.4). The greatest percent difference for kfadmm was larger for the 20-story structure than the 9-story structure, 6.101 percent compared to 3.813.

2. The kfadmm algorithm required fewer total function evaluations than the exact and sequential methods (Tables 6.3 and 6.5), allowing for a computationally less expensive way for users to know the performance lost due to having one less sensor before deciding whether or not to exclude that sensor.

Table 6.4: $\mathrm{tr}\left(\mathbf{P}_{k|k}\right)$ percent difference comparison with the exact method for acceleration sensor selections made with the sequential and kfadmm methods, assuming $\mathbf{Q}/\mathbf{R} < 1$ for the 20-story nonlinear benchmark structure

$\mathrm{tr}\left(\mathbf{P}_{k\|k}\right)$ Percent Difference for **No.** of Sensors	Sequential	kfadmm
19	0	0
18	0	0.167
17	0	0.292
16	0	0.328
15	0	1.025
14	0	2.024
13	0.017	1.954
12	0.082	1.822
11	0.167	2.490
10	0.098	3.866
9	0.087	4.173
8	0.075	4.902
7	0.018	5.753
6	0	6.101
5	0.065	5.864
4	0.120	2.878
3	0.140	1.962
2	0	0.989
1	0	0

Table 6.5: Comparison of number of function evaluations for a certain number of selected acceleration sensors, assuming $\mathbf{Q}/\mathbf{R} < 1$, for the exact, sequential, and kfadmm methods applied to the 20-story nonlinear benchmark structure

Method		Exact	Sequential	kfadmm
Function Evaluations for **No.** of Sensors	**19**	20	209	261
	18	190	207	287
	17	1,140	204	301
	16	4,845	200	324
	15	15,504	195	350
	14	38,760	189	369
	13	77,520	182	379
	12	125,970	174	407
	11	167,960	165	415
	10	184,756	155	422
	9	167,960	144	499
	8	125,970	132	600
	7	77,520	119	714
	6	38,760	105	753
	5	15,504	90	814
	4	4,845	74	1,164
	3	1,140	57	1,268
	2	190	39	1,483
	1	20	20	2,240
Total Evaluations		1,048,574	2,660	2,240

6.3 Impact of Model Type: Reduced-order versus Shear

The sensor selections for the shear models differed from those of the reduced-order models. As an example, compare the results for the 9-story structure in Table 6.6. The selections for a single sensor all match, selecting the 9th-floor sensor; however, the remaining selections are model-dependent. When comparing the shear model selections made by kfadmm to those made by the exact and sequential methods, kfadmm still resulted in similar sensor selections for the 3- and 9- story models. In fact, for the 9-story shear model with $\mathbf{Q}/\mathbf{R} < 1$, the kfadmm, sequential, and exact choices all matched, as can be seen in Table 6.6. Matching sensor choices meant equivalent costs; thus, the number of function evaluations was the best way to evaluate the selection algorithms. Table 6.7 shows that, as with the reduced-order model, the kfadmm method required

significantly fewer total evaluations than the exact and sequential methods for the shear building model. The 20-story shear models showed less agreement among the selection methods (Tables A.12 - A.15), unearthing a potential limitation of the kfadmm method that may need to be addressed in future work.

Table 6.6: Comparison of acceleration sensor selection results, assuming $\mathbf{Q/R} < 1$, for the reduced-order and shear models of the 9-story nonlinear benchmark structure

Model Type	Method	Exact Selection (Floors)	Sequential Selection (Floors)	kfadmm Selection (Floors)
Reduced-order	**No.** of Sensors **8**	9 8 7 6 4 3 2 1	9 8 7 6 5 3 2 1	9 7 6 5 4 3 2 1
	7	9 8 6 5 3 2 1	9 8 6 5 3 2 1	9 6 5 4 3 2 1
	6	9 8 6 5 3 2	9 8 6 5 3 2	9 5 4 3 2 1
	5	9 8 6 3 2	9 8 6 3 2	9 4 3 2 1
	4	9 8 3 2	9 8 6 3	9 3 2 1
	3	9 8 2	9 6 3	9 2 1
	2	9 6	9 6	
	1	9	9	9
Shear	**No.** of Sensors **8**	9 8 7 6 5 4 3 2	9 8 7 6 5 4 3 2	9 8 7 6 5 4 3 2
	7	9 8 7 6 5 4 3	9 8 7 6 5 4 3	9 8 7 6 5 4 3
	6	9 8 7 6 5 4	9 8 7 6 5 4	9 8 7 6 5 4
	5	9 8 7 6 5	9 8 7 6 5	9 8 7 6 5
	4	9 8 7 6	9 8 7 6	9 8 7 6
	3	9 8 7	9 8 7	9 8 7
	2	9 8	9 8	9 8
	1	9	9	9

Table 6.7: Comparison of number of function evaluations for a certain number of selected acceleration sensors, assuming $\mathbf{Q/R} < 1$, for the exact, sequential, and kfadmm methods applied to the 9-story nonlinear shear structure

Method	Function Evaluations for **No.** of Sensors								**Total**
	8	**7**	**6**	**5**	**4**	**3**	**2**	**1**	**Evaluations**
Exact	9	36	84	126	126	84	36	9	510
Sequential	44	42	39	35	30	24	17	9	240
kfadmm	10	16	22	28	34	39	43	46	46

6.4 Summary

Independent of system scale and model type, the kfadmm algorithm resulted in similar sensor selections to the exact and sequential placement methods. However, it bettered previous placement methods because it provided an efficient means of determining the "best" number of sensors, requiring fewer total evaluations to choose the desired number of sensors based on a known degree of sub-optimality.

Chapter 7

Effect of Covariance Weightings on Sensor Selection

Over the course of this research, the covariances $\mathbf{R}$ and $\mathbf{Q}$, relating the measurement and process noise respectively, were observed to impact the sensor selection results for all three sensor selection methods considered.

Using the 9-story nonlinear benchmark as an example, the sensor selection results assuming one trusts the measurements more than the model, $\mathbf{Q}/\mathbf{R} > 1$, for the exact, sequential, and kfadmm methods are shown in Table 7.1. Note that, as labeled, all previous results presented assumed that the system and disturbance model was trusted more than the measurements, $\mathbf{Q}/\mathbf{R} < 1$. The selection results depended on whether there was more uncertainty in the measurements or the model and disturbance. While these results are only shown here for the 9-story benchmark, they were observed for the other benchmark structures as well. The selection results for all of the models considered are detailed in Appendix A. For $\mathbf{Q}/\mathbf{R} < 1$, a system in which the measurements are assumed noisier than the model, the 9th-floor sensor was selected. The 9th-floor sensor gives more information about the system response when the system and disturbance model is trusted more. On the other hand, for $\mathbf{Q}/\mathbf{R} \geq 1$, a system in which one trusts the measurements as much as or more than the model, the sensor selection algorithms ultimately selected the first-floor sensor. The hypothesis behind the first-floor sensor selection is that this sensor provides more information about the excitation at ground level, which is valuable information to combine with the measurements for estimate correction.

Table 7.1: Comparison of acceleration sensor selection results, assuming $\mathbf{Q}/\mathbf{R} > 1$ ($\mathbf{Q}/\mathbf{R} = 100$), for the exact, sequential, and kfadmm methods applied to the 9-story nonlinear benchmark structure

Method		Exact Selection (Floors)								Sequential Selection (Floors)								kfadmm Selection (Floors)							
No. of Sensors	**8**	9	7	6	5	4	3	2	1	9	7	6	5	4	3	2	1								
	7	9		6	5	4	3	2	1	9		6	5	4	3	2	1								
	6	9			5	4	3	2	1	9			5	4	3	2	1		6	5	4	3	2	1	
	5	9				4	3	2	1	9				4	3	2	1			5	4	3	2	1	
	4	9					3	2	1	9				4		2	1				4	3	2	1	
	3	9						2	1					4		2	1					3	2	1	
	2					4			1					4			1						2	1	
	1								1								1								1

Note that for the 9-story nonlinear benchmark structure with $\mathbf{Q}/\mathbf{R} > 1$ the kfadmm placement method did not select a combination of eight or seven sensors. The hypothesis behind this result is that the Euclidean norms of the columns corresponding to floors 7, 8, and 9 were so similar the algorithm did not differentiate between them for the employed γ range.

Chapter 8

Conclusions and Future Research

8.1 Summary of Key Conclusions

This thesis proposes the Kalman filter alternating direction method of multipliers (kfadmm) algorithm to systematically balance measurement sparsity and estimator error covariance in acceleration sensor selection for civil structures.

Independent of system scale and model type, the kfadmm algorithm results in similar sensor selections to the exact and sequential placement methods while offering only slightly sub-optimal performance. The kfadmm algorithm also allows for more flexibility in the sensor selection problem. It was shown that with kfadmm, the choice of m sensors for a given system can be made after knowing how much each additional sensor contributes to the estimation performance. Moreover, because users have control over the sparsity parameter, γ, kfadmm has the potential to greatly reduce the number of function evaluations required to determine sensor placement.

An interesting observation is that the covariance weightings affect sensor selection. When the model is trusted more than the measurements, the nth-floor sensor of an n-floor structure excited at the ground matters most; however, when the measurements are trusted more than the model, the first-floor sensor controls the estimator design.

8.2 Recommended Future Research

In the future, both algorithm improvement and selection results should be explored. The effects of softening the penalty function, $\mathbf{g}(\mathbf{L})$, should be investigated. Perhaps a weighted l_1 approach could be used to shrink the gain matrix and maintain a convex

optimization problem. The potential limitation with the kfadmm method discovered through evaluation of the 20-story shear models might be addressed with the use of a different norm in the ADMM. The Euclidean norm appears to work well with the reduced-order models, so one challenge with considering different norm functions would be finding a substitution that is robust enough to accommodate selection for any model considered. Another goal would be to quantify how many sensors make a significant impact on overall performance when the assumed noise characteristics are violated. Additionally, applying the kfadmm approach to incorporate multiple measurements, beyond acceleration, would allow for characterization of the impact of measurement type on selection. Furthermore, simulating the response of a structure subjected to an earthquake record and implementing the sensor selections would show how well the sparse measurement systems compare both among methods as well as to a system with full measurement feedback.

References

[Abdullah et al., 2000] Abdullah, M. M., Richardson, A., and Hanif, J. (2000). Placement of sensors/actuators on civil structures using genetic algorithms. *Earthquake Engineering and Structural Dynamics*, 30(8):1167–1184.

[Chen, 2013] Chen, L. L. T. (2013). What can regularization offer for estimation of dynamical systems? *IFAC Proceedings Volumes*, 46(11):1–8.

[Giraud and Jouvencel, 1995] Giraud, C. and Jouvencel, B. (1995). Sensor selection: A geometrical approach. volume 2. IEEE/RSJ Int. Conf. Intelligent Robot Systems.

[Hernandez, 2017] Hernandez, E. M. (2017). Efficient sensor placement for state estimation in structural dynamics. *Mechanical Systems and Signal Processing*, 85:789–800.

[Hinson, 2014] Hinson, B. T. (2014). *Observability-Based Guidance and Sensor Placement*. PhD thesis, University of Washington.

[Joshi and Boyd, 2009] Joshi, S. and Boyd, S. (2009). Sensor selection via convex optimization. *IEEE Transactions on Signal Processing*, 57(2):451–462.

[Kammer, 2005] Kammer, D. (2005). Sensor set expansion for modal vibration testing. *Mechanical Systems and Signal Processing*, 19(4):700–713.

[Lin et al., 2013] Lin, F., Fardad, M., and Jovanovic, M. R. (2013). Design of optimal sparse feedback gains via the alternating direction method of multipliers. *IEEE Transactions on Automatic Control*, 58(9):2426–2431.

[Ohtori et al., 2004] Ohtori, Y., Christenson, R. E., Spencer Jr., B. F., and Dyke, S. J. (2004). Benchmark control problems for seismically excited nonlinear buildings. *Journal of Engineering Mechanics Special Issue: Benchmark Structural Control Problem*, 130:366–385.

[Papadimitriou, 2003] Papadimitriou, C. (2003). Optimal sensor placement methodology for parametric identification of structural systems. *Journal of Sound and Vibration*, 278:923–947.

[Papadimitriou and Lombaert, 2012] Papadimitriou, C. and Lombaert, G. (2012). The effect of prediction error correlation on optimal sensor placement in structural dynamics. *Mechanical Systems and Signal Processing*, 28(C):105–127.

[Sun et al., 2015] Sun, H., Feng, D., Liu, Y., and Feng, M. Q. (2015). Statistical regularization for identification of structural parameters and external loadings using state space models. *Computer-Aided Civil and Infrastructure Engineering*, 30:843–858.

[Sun et al., 2016] Sun, Z., Li, B., Dyke, S., Lu, C., and Linderman, L. (2016). Benchmark problem in active structural control with wireless sensor network. *Structural Control and Health Monitoring*, 23:20–34.

[Tan et al., 2005] Tan, P., Dyke, S. J., Richardson, A., and Abdullah, M. (2005). Integrated device placement and control design in civil structures using genetic algorithms. *Journal of Structural Engineering*, 131(10):1489–1496.

[Thacker and Lacey, 1998] Thacker, N. A. and Lacey, A. J. (1998). *Tutorial: The Likelihood Interpretation of the Kalman Filter*. Tina Memo No. 1996-002, University of Manchester.

[The MathWorks, Inc., 2018] The MathWorks, Inc. (2018). Matlab and control system toolbox release 2018b.

[Van Der Linden et al., 2011] Van Der Linden, G., Emami-Naeini, A., Kosut, R., Sedarat, H., and Lynch, J. (2011). Optimal sensor placement for health monitoring of civil structures. In *Proceedings of the American Control Conference*, pages 3116–3121.

[Yao, 1998] Yao, J. T. P. (1998). Concept of structural control. *Journal of Structural Division, ASCE*, 7:1567–1574.

[Yao et al., 1992] Yao, L., Sethares, W. A., and Kammer, D. C. (1992). Sensor placement for on-orbit modal identification of large space structure via a genetic algorithm. IEEE International Conference on Systems Engineering.

[Zhang and Xu, 2016] Zhang, C. and Xu, Y. (2016). Optimal multi-type sensor placement for response and excitation reconstruction. *Journal of Sound and Vibration*, 360:112–128.

Appendix A

Tabulated Sensor Selections

Appendix A details the comparison of sensor selection results for the exact, sequential, and kfadmm methods when applied to the various models considered.

A.1 3-story Wireless Benchmark

Table A.1: 3-story wireless benchmark $\mathbf{Q}/\mathbf{R} < 1$

Method		**No.** of Sensors		
		3	**2**	**1**
Exact	Selection (Floors)	3	3	3
		2	2	
		1		
Sequential	Selection (Floors)	3	3	3
		2	2	
		1		
kfadmm	Selection (Floors)	3	3	3
		2	2	
		1		

Table A.2: 3-story wireless benchmark $\mathbf{Q}/\mathbf{R} > 1$

Method		**No.** of Sensors		
		3	**2**	**1**
Exact	Selection (Floors)	3	3	
		2		
		1	1	1
Sequential	Selection (Floors)	3	3	
		2		
		1	1	1
kfadmm	Selection (Floors)	AMD	AMD	
		3		
		1	1	1

A.2 3-story Nonlinear Benchmark

Table A.3: 3-story nonlinear benchmark reduced-order model $\mathbf{Q}/\mathbf{R} < 1$

Method		**No.** of Sensors	
		2	**1**
Exact	Selection (Floors)	3	3
		2	
Sequential	Selection (Floors)	3	3
		2	
kfadmm	Selection (Floors)		3

Table A.4: 3-story nonlinear benchmark reduced-order model $\mathbf{Q/R} > 1$

Method		**No.** of Sensors	
		2	**1**
Exact	Selection (Floors)	2	
		1	1
Sequential	Selection (Floors)	2	
		1	1
kfadmm	Selection (Floors)	2	
		1	1

Table A.5: 3-story nonlinear benchmark shear model $\mathbf{Q/R} < 1$

Method		**No.** of Sensors	
		2	**1**
Exact	Selection (Floors)	3	3
		2	
Sequential	Selection (Floors)	3	3
		2	
kfadmm	Selection (Floors)	3	3
		2	

Table A.6: 3-story nonlinear benchmark shear model $\mathbf{Q/R} > 1$

Method		**No.** of Sensors	
		2	**1**
Exact	Selection (Floors)	3	
		1	1
Sequential	Selection (Floors)	3	
		1	1
kfadmm	Selection (Floors)	3	
		1	1

A.3 9-story Nonlinear Benchmark

Table A.7: 9-story nonlinear benchmark shear model $\mathbf{Q/R} > 1$

Method		Exact Selection (Floors)	Sequential Selection (Floors)	kfadmm Selection (Floors)
No. of Sensors	**8**	9 8 7 5 4 3 2 1	9 8 6 5 4 3 2 1	8 7 6 5 4 3 2 1
	7	9 8 6 4 3 2 1	9 8 6 4 3 2 1	7 6 5 4 3 2 1
	6	9 7 5 3 2 1	9 8 6 3 2 1	6 5 4 3 2 1
	5	9 6 3 2 1	8 6 3 2 1	5 4 3 2 1
	4	9 5 2 1	8 6 3 1	4 3 2 1
	3	8 3 1	8 3 1	3 2 1
	2	8 1	3 1	2 1
	1	3	3	1

A.4 20-story Nonlinear Benchmark

Table A.8: 20-story nonlinear benchmark reduced-order model $\mathbf{Q/R} < 1$

Method		**No.** of Sensors																	
		19	**18**	**17**	**16**	**15**	**14**	**13**	**12**	**11**	**10**	**9**	**8**	**7**	**6**	**5**	**4**	**3**	**2**	**1**
Exact	Selection (Floors)	20	20	20	20	20	20	20	20	20	20	20	20	20	20	20	20	20	20	20
		19	19	19	19	19	19								19		19			
		18	18	18	18	18	18	18	18	18	18	18	18	18		18		18		
		17	17	17	17	17	17	17	17	17	17	17	17	17	17				17	
		16	16	16																
		14																		
		13	13	13	13	13	13	13	13	13	13									
		12	12	12	12	12	12	12	12											
		11	11	11	11															
		10	10																	
		9	9	9	9	9														
		8	8	8	8	8	8	8	8	8	8	8								
		7	7	7	7	7	7	7	7	7	7	7	7	7	7	7				
		6	6	6	6	6	6	6	6	6	6	6	6							
		5	5	5	5	5	5	5	5	5										
		4	4	4	4	4	4	4	4	4	4	4	4	4						
		3	3	3	3	3	3	3	3	3	3	3	3	3	3	3	3	3		
		2	2	2	2	2	2	2	2	2	2	2	2	2	2	2	2			
		1	1	1	1	1	1	1												
Sequential	Selection (Floors)	20	20	20	20	20	20	20	20	20	20	20	20	20	20	20	20	20	20	20
		19	19	19	19	19	19	19	19	19	19	19	19	19	19					
		18	18	18	18	18	18	18	18											
		17	17	17	17	17	17	17	17	17	17	17	17	17	17	17	17	17	17	
		16	16	16																
		14																		
		13	13	13	13	13	13	13	13	13	13									
		12	12	12	12	12	12													
		11	11	11	11															
		10	10																	
		9	9	9	9	9														
		8	8	8	8	8	8	8	8	8	8	8	8							
		7	7	7	7	7	7	7	7	7	7	7	7	7	7	7	7			
		6	6	6	6	6	6	6	6	6	6	6								
		5	5	5	5	5	5	5	5	5										
		4	4	4	4	4	4	4	4	4	4	4	4	4						
		3	3	3	3	3	3	3	3	3	3	3	3	3	3	3	3	3		
		2	2	2	2	2	2	2	2	2	2	2	2	2	2	2	2			
		1	1	1	1	1	1	1												

Table A.9: 20-story nonlinear benchmark reduced-order model $\mathbf{Q/R} < 1$ cont.

Method	**No.** of Sensors																	
	19	**18**	**17**	**16**	**15**	**14**	**13**	**12**	**11**	**10**	**9**	**8**	**7**	**6**	**5**	**4**	**3**	**2**	**1**
kfadmm	20	20	20	20	20	20	20	20	20	20	20	20	20	20	20	20	20	20	20
	19																		
	18	18	18	18															
	17	17	17	17	17														
	16	16																	
	14	14	14																
	13	13	13	13	13	13	13	13	13										
	12	12	12	12	12	12	12	12											
	11	11	11	11	11	11													
	10	10	10	10	10	10	10												
	9	9	9	9	9	9	9	9	9	9									
	8	8	8	8	8	8	8	8	8	8	8								
	7	7	7	7	7	7	7	7	7	7	7	7							
	6	6	6	6	6	6	6	6	6	6	6	6	6						
	5	5	5	5	5	5	5	5	5	5	5	5	5	5					
	4	4	4	4	4	4	4	4	4	4	4	4	4	4	4	4			
	3	3	3	3	3	3	3	3	3	3	3	3	3	3	3	3	3		
	2	2	2	2	2	2	2	2	2	2	2	2	2	2	2	2	2	2	
	1	1	1	1	1	1	1	1	1	1	1	1	1	1	1				

Selection (Floors)

Table A.10: 20-story nonlinear benchmark reduced-order model $\mathbf{Q/R} > 1$

Method	**No.** of Sensors																		
	19	**18**	**17**	**16**	**15**	**14**	**13**	**12**	**11**	**10**	**9**	**8**	**7**	**6**	**5**	**4**	**3**	**2**	**1**
Exact	20	20	20	20	20	20	20	20	20	20	20	20	20	20	20	20	20		
Selection (Floors)	18	18	18	18	18	18	18												
	17	17																	
	16	16	16																
	15																		
	14	14	14	14															
	13	13	13	13	13														
	12	12	12	12	12	12													
	11	11	11	11	11	11	11	11	11										
	10	10	10	10	10	10	10	10											
	9	9	9	9	9	9	9	9	9	9									
	8	8	8	8	8	8	8	8	8	8	8	8							
	7	7	7	7	7	7	7	7	7	7	7								
	6	6	6	6	6	6	6	6	6	6	6	6	6	6					
	5	5	5	5	5	5	5	5	5	5	5	5	5						
	4	4	4	4	4	4	4	4	4	4	4	4	4	4	4				
	3	3	3	3	3	3	3	3	3	3	3	3	3	3	3		3		
	2	2	2	2	2	2	2	2	2	2	2	2	2	2	2	2	2		
	1	1	1	1	1	1	1	1	1	1	1	1	1	1	1	1	1	1	1
Sequential	20	20	20	20	20	20	20	20	20	20	20	20	20	20	20	20	20		
Selection (Floors)	18	18	18	18	18	18	18												
	17	17																	
	16	16	16																
	15																		
	14	14	14	14															
	13	13	13	13	13														
	12	12	12	12	12	12													
	11	11	11	11	11	11	11	11	11										
	10	10	10	10	10	10	10	10											
	9	9	9	9	9	9	9	9	9	9									
	8	8	8	8	8	8	8	8	8	8	8	8							
	7	7	7	7	7	7	7	7	7	7	7								
	6	6	6	6	6	6	6	6	6	6	6	6	6	6					
	5	5	5	5	5	5	5	5	5	5	5	5	5						
	4	4	4	4	4	4	4	4	4	4	4	4	4	4	4				
	3	3	3	3	3	3	3	3	3	3	3	3	3	3	3	3	3	3	
	2	2	2	2	2	2	2	2	2	2	2	2	2	2	2	2			
	1	1	1	1	1	1	1	1	1	1	1	1	1	1	1	1	1	1	1

Table A.11: 20-story nonlinear benchmark reduced-order model $\mathbf{Q}/\mathbf{R} > 1$ cont.

Method	**No.** of Sensors																		
	19	**18**	**17**	**16**	**15**	**14**	**13**	**12**	**11**	**10**	**9**	**8**	**7**	**6**	**5**	**4**	**3**	**2**	**1**
kfadmm	20	20																	
	19																		
	17	17	17																
	16	16	16	16															
	15	15	15	15	15														
	14	14	14	14	14	14	14	14											
	13	13	13	13	13	13													
	12	12	12	12	12	12	12	12	12										
	11	11	11	11	11	11	11	11	11	11									
	10	10	10	10	10	10	10												
	9	9	9	9	9	9	9	9	9	9	9	9	9						
	8	8	8	8	8	8	8	8	8	8	8	8	8	8					
	7	7	7	7	7	7	7	7	7	7	7	7							
	6	6	6	6	6	6	6	6	6	6	6	6	6	6	6	6			
	5	5	5	5	5	5	5	5	5	5	5								
	4	4	4	4	4	4	4	4	4	4	4	4	4	4	4	4	4	4	
	3	3	3	3	3	3	3	3	3	3	3	3	3	3	3				
	2	2	2	2	2	2	2	2	2	2	2	2	2	2	2	2	2		
	1	1	1	1	1	1	1	1	1	1	1	1	1	1	1	1	1	1	1

Selection (Floors)

Table A.12: 20-story nonlinear benchmark shear model $\mathbf{Q/R} < 1$

Method	**No.** of Sensors																		
	19	**18**	**17**	**16**	**15**	**14**	**13**	**12**	**11**	**10**	**9**	**8**	**7**	**6**	**5**	**4**	**3**	**2**	**1**
Exact	20	20	20	20	20	20	20	20	20	20	20	20	20	20	20	20	20	20	20
	19	19	19	19	19	19	19	19	19	19	19	19	19	19	19	19	19	19	
	18	18	18	18	18	18	18	18	18	18	18	18	18	18	18				
	17	17	17	17	17	17	17	17	17	17	17	17				17			
	16	16	16	16	16	16	16	16	16	16	16		16						
	15	15	15	15	15	15	15	15	15					15			15		
	14	14	14	14	14	14	14	14		14		14	14		14				
	13	13	13	13	13	13	13		13	13	13	13		13		13			
	12	12	12	12	12	12		12	12		12				12				
	11	11	11	11	11		11						11	11					
	10	10	10	10		10		10		10		10	10						
	9	9	9		9		9	9	9	9	9	9							
	8	8		8		8	8		8		8								
					7														
	6		6			6		6		6									
	5	5							5										
	4	4	4	4	4		4	4											
	3	3	3	3		3	3												
	2	2	2	2	2														
	1	1	1	1	1	1													
Sequential	20	20	20	20	20	20	20	20	20	20	20	20	20	20	20	20	20	20	20
	19	19	19	19	19	19	19	19	19	19	19	19	19	19	19	19	19	19	
	18	18	18	18	18	18	18	18	18	18	18	18	18	18					
	17	17	17	17	17	17	17	17	17	17	17								
	16	16	16	16	16	16	16	16	16										
	15	15	15	15	15	15	15	15	15	15	15	15	15	15	15	15	15		
	14	14	14	14	14	14	14	14	14	14	14	14	14	14	14	14			
	13	13	13	13	13	13													
	12	12	12	12	12	12	12	12	12	12	12	12	12	12	12				
	11	11	11	11															
	10	10	10	10	10	10	10	10	10	10	10	10	10						
	9	9	9	9	9	9	9	9	9	9	9	9							
	8	8																	
	6	6	6	6	6	6	6	6	6	6									
	5																		
	4	4	4	4	4	4	4	4											
	3	3	3																
	2	2	2	2	2														
	1	1	1	1	1	1	1												

Selection (Floors)

Table A.13: 20-story nonlinear benchmark shear model $\mathbf{Q/R} < 1$ cont.

Method	**No.** of Sensors																	
	19	**18**	**17**	**16**	**15**	**14**	**13**	**12**	**11**	**10**	**9**	**8**	**7**	**6**	**5**	**4**	**3**	**2**	**1**
kfadmm	20	20	20	20	20	20	20	20	20	20	20	20	20	20	20	20	20	20	20
	19	19	19	19	19	19	19	19	19	19	19	19	19	19	19	19	19	19	
	18	18	18	18	18	18	18	18	18	18	18	18	18	18	18	18	18		
	17	17	17	17	17	17	17	17	17	17	17	17	17	17	17	17			
	16	16	16	16	16	16	16	16	16	16	16	16	16	16	16				
	15	15	15	15	15	15	15	15	15	15	15	15	15	15					
	14	14	14	14	14	14	14	14	14	14	14	14	14						
	13	13	13	13	13	13	13	13	13	13	13	13							
	12	12	12	12	12	12	12	12	12	12	12								
	11	11	11	11	11	11	11	11	11	11									
	10	10	10	10	10	10	10	10	10										
	9	9	9	9	9	9	9	9											
	8	8	8	8	8	8	8												
	7	7	7	7	7	7													
	6	6	6	6	6														
	5	5	5	5															
	4	4	4																
	3	3																	
	2																		

Selection (Floors)

Table A.14: 20-story nonlinear benchmark shear model $\mathbf{Q/R} > 1$

Method	**No.** of Sensors																		
	19	**18**	**17**	**16**	**15**	**14**	**13**	**12**	**11**	**10**	**9**	**8**	**7**	**6**	**5**	**4**	**3**	**2**	**1**
Exact	20	20	20	20	20	20	20	20	20	20	20	20	20	20	20				
	19	19	19	19	19	19	19	19	19	19						19	19		
	18	18	18	18	18	18	18				18	18							
	17	17	17	17	17			17	17				17					17	
	16	16	16			16	16			16				16					
	15	15		15	15			15			15								
	14		14	14		14			14			14			14				
	13	13	13		13		13	13		13									
		12		12		12	12		12		12		12			12			
	11		11		11									11					
	10	10		10		10		10		10		10							
	9	9	9		9														
	8	8	8	8			8		8										
	7	7	7	7	7	7													
	6	6	6	6	6	6	6	6											
	5	5	5	5	5	5	5	5	5	5	5								5
	4	4	4	4	4	4	4	4	4	4	4	4	4				4		
	3	3	3	3	3	3	3	3	3	3	3	3	3	3	3				
	2	2	2	2	2	2	2	2	2	2	2	2	2	2	2	2			
	1	1	1	1	1	1	1	1	1	1	1	1	1	1	1	1	1	1	
Sequential	20	20	20	20	20	20	20	20	20	20	20								
	19	19	19	19	19	19	19	19	19	19	19	19	19	19	19	19	19		
	18	18	18	18															
	17	17	17	17	17	17	17	17											
	16	16	16	16	16	16	16	16	16	16	16	16	16	16					
	15																		
	14	14	14	14	14	14													
	13	13	13	13	13	13	13	13	13	13	13	13	13	13	13	13			
	12	12																	
	10	10	10	10	10	10	10	10	10	10	10	10							
	9	9	9	9	9	9	9												
	8	8	8																
	7	7	7	7	7														
	6	6	6	6	6	6	6	6	6										
	5	5	5	5	5	5	5	5	5	5	5	5	5	5	5	5	5	5	5
	4	4	4	4	4	4	4	4	4	4									
	3	3	3	3	3	3	3	3	3	3	3	3	3						
	2	2	2	2	2	2	2	2	2	2	2	2	2	2	2				
	1	1	1	1	1	1	1	1	1	1	1	1	1	1	1	1	1	1	

Selection (Floors)

Table A.15: 20-story nonlinear benchmark shear model $\mathbf{Q/R} > 1$ cont.

Method	**No.** of Sensors																		
	19	**18**	**17**	**16**	**15**	**14**	**13**	**12**	**11**	**10**	**9**	**8**	**7**	**6**	**5**	**4**	**3**	**2**	**1**
kfadmm																			
Selection (Floors)	19																		
	18	18																	
	17	17	17																
	16	16	16	16															
	15	15	15	15	15														
	14	14	14	14	14	14													
	13	13	13	13	13	13	13												
	12	12	12	12	12	12	12	12											
	11	11	11	11	11	11	11	11	11										
	10	10	10	10	10	10	10	10	10	10									
	9	9	9	9	9	9	9	9	9	9	9								
	8	8	8	8	8	8	8	8	8	8	8	8							
	7	7	7	7	7	7	7	7	7	7	7	7	7						
	6	6	6	6	6	6	6	6	6	6	6	6	6	6					
	5	5	5	5	5	5	5	5	5	5	5	5	5	5	5				
	4	4	4	4	4	4	4	4	4	4	4	4	4	4	4	4			
	3	3	3	3	3	3	3	3	3	3	3	3	3	3	3	3	3		
	2	2	2	2	2	2	2	2	2	2	2	2	2	2	2	2	2	2	
	1	1	1	1	1	1	1	1	1	1	1	1	1	1	1	1	1	1	1

Appendix B

Selection and Implications of γ Range

Users have significant freedom in terms of selecting the sparsity parameter, γ, which appears in the objective function of the kfadmm sensor selection algorithm (Equation 4.1). However, with that freedom can also come confusion as to how γ is actually affecting the selection process. This appendix points to a few important findings regarding the γ range to aid those who may wish to implement the algorithm in the future.

B.1 Selection of γ Range

The user-specified γ range consists of three components: a starting value, an ending value, and an increment value to step between the two former elements. The starting value in this work was always assumed to be zero. The ending value differed depending on the model, but some quick cycling through the algorithm provided a means of determining an ending value without significant effort. The increment value could be tricky, however, because it directly affected the quantity of function evaluations and quality of sensor selections. A method for selecting the increment value is discussed below.

The 20-story nonlinear reduced-order model will be used to introduce a means of determining if an initial guess for the increment value provides accurate results. Table A.9 contains the sensor selections for $\gamma = [0 : 1 * 10^{-6} : 2.3 * 10^{-3}]$. Table B.1 illustrates that increasing the γ increment value to $1 * 10^{-5}$, which corresponds to decreasing the quantity of function evaluations, dramatically changes the sensor selection results.

Table B.1: Acceleration sensor selection results, assuming $\mathbf{Q}/\mathbf{R} < 1$, for the 20-story nonlinear benchmark structure and implementing a coarse γ range

Method	**No.** of Sensors																			
	19	**18**	**17**	**16**	**15**	**14**	**13**	**12**	**11**	**10**	**9**	**8**	**7**	**6**	**5**	**4**	**3**	**2**	**1**
kfadmm	20	20	20	20	20	20	20	20		20	20	20							
	19																		
	18	18	18	18															
	17	17	17	17	17														
	16	16																	
	14	14	14																
	13	13	13	13	13	13	13	13											
	12	12	12	12	12	12	12	12											
	11	11	11	11	11	11													
	10	10	10	10	10	10	10												
	9	9	9	9	9	9	9	9		9									
	8	8	8	8	8	8	8	8		8	8								
	7	7	7	7	7	7	7	7		7	7	7	7						
	6	6	6	6	6	6	6	6		6	6	6	6	6					
	5	5	5	5	5	5	5	5		5	5	5	5	5	5				
	4	4	4	4	4	4	4	4		4	4	4	4	4	4	4			
	3	3	3	3	3	3	3	3		3	3	3	3	3	3	3	3	3	
	2	2	2	2	2	2	2	2		2	2	2	2	2	2	2	2	2	2
	1	1	1	1	1	1	1	1		1	1	1	1	1	1	1	1		

Selection (Floors)

If we compare the kfadmm results in Tables A.9 and B.1 to Table A.8 containing the exact and sequential method results, it is clear that the selections in Table A.9 more closely match the choices from the other algorithms. The degree of sub-optimality of the kfadmm sensor selections was greater when the coarser γ range was used. A comparison of the covariance estimation error for the various methods, including when kfadmm was run for the two different γ ranges, is shown in Figure B.1.

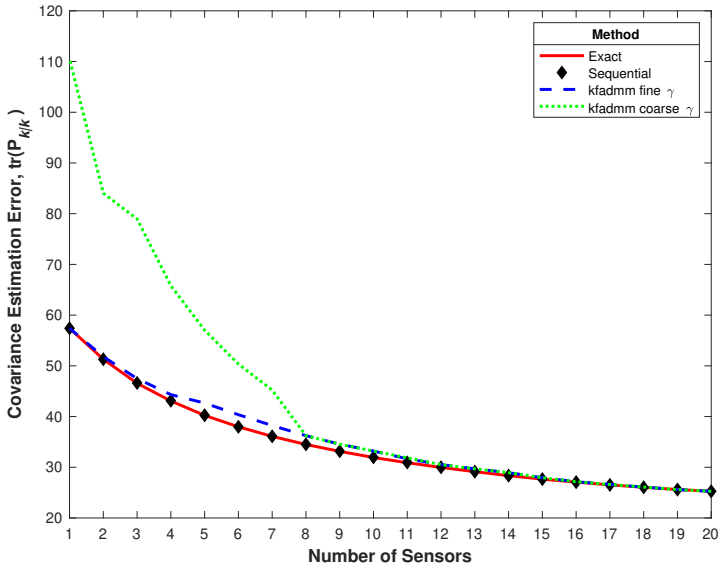

Figure B.1: Comparison of $\mathrm{tr}\,(\mathbf{P}_{k|k})$ for different γ ranges applied to the 20-story nonlinear benchmark structure

In the case of the 20-story nonlinear benchmark structure, the increment value not only had the potential to change the sensor selection results but also impacted the degree of sub-optimality of the sensor selections. One of the main differences in the sensor selections for the different γ ranges was in the selection of one sensor: the finer γ range selected the 20th-floor sensor (matching the exact and sequential results) whereas the coarser range chose the 2nd-floor sensor. To determine if an increment value is fine enough, compare the kfadmm results for selecting one sensor to the results for one sensor selected through the exact or sequential method. As is shown in Table 6.5, a one-sensor selection from the exact or sequential method would only require considering twenty additional function evaluations, thus not significantly increasing the computational effort.

B.2 Implications of γ Range on Number of Function Evaluations

An important implication of the γ range is that the choice of γ can result in more or fewer function evaluations. It is important to understand when and how to alter γ in

order for the kfadmm algorithm to reduce the number of function evaluations.

Recall the sensor selections for the 9-story nonlinear benchmark presented in Table 6.1 and the corresponding numbers of function evaluations from Table 6.3. Considering the selections for three sensors as an example, one observes that the kfadmm method outperformed the exact method in requiring fewer function evaluations (31 compared to 84); however, the kfadmm method still required more evaluations than the sequential method (31 compared to 24). For this example, a fine γ range was chosen in order to compare the sensor selections for most of the possible numbers of sensors. If one wanted to decrease the number of required function evaluations or did not need as much information about all of the possible placements, a coarser γ range could be implemented. A comparison of the selection results for $\gamma = [0 : 1 * 10^{-5} : 3.5 * 10^{-4}]$ (fine) and $\gamma = [0 : 2.5 * 10^{-5} : 3.5 * 10^{-4}]$ (coarse) are seen in Table B.2.

Table B.2: Comparison of acceleration sensor selection results, assuming $\mathbf{Q}/\mathbf{R} < 1$, for fine and coarse γ ranges applied to the 9-story nonlinear benchmark structure

γ Range	**No.** of Sensors	Selection (Floors)							
Fine	**8**	9	7	6	5	4	3	2	1
	7	9		6	5	4	3	2	1
	6	9			5	4	3	2	1
	5	9				4	3	2	1
	4	9					3	2	1
	3	9						2	1
	1	9							
Coarse	**8**								
	7	9		6	5	4	3	2	1
	6								
	5	9				4	3	2	1
	4	9					3	2	1
	3	9						2	1
	1	9							

Notice that in the case of this 9-story model, a coarser γ range resulted in choices for fewer of the possible number of sensors: there were no results for 6 or 8 sensors; however, unlike the 20-story phenomenon explored above, the actual sensor choices remained the same as with the finer γ range. For selecting three sensors, this coarser γ range required only 13 function evaluations, fewer than both the exact and sequential methods.